

# Estimates of the thermal conductivity and the thermoelectric properties of $\text{PbTiO}_3$ from first principles

Anindya Roy\*

Materials Science & Engineering, Johns Hopkins University, Baltimore, MD 21218, USA

(Dated: September 30, 2015)

The lattice thermal conductivity ( $\kappa_L$ ) of  $\text{PbTiO}_3$  (PTO) is estimated using a combination of *ab initio* calculations and semiclassical Boltzmann transport equation. The computed  $\kappa_L$  is remarkably low, nearly comparable with the  $\kappa_L$  of good thermoelectric materials such as  $\text{PbTe}$ . In addition, a semiclassical analysis of the electronic transport quantities is presented, which suggests excellent thermoelectric properties, with a figure of merit  $zT$  well over 1 for a wide range of temperature. For thermoelectric applications, the  $\kappa_L$  could be further reduced by utilizing different morphologies and compositions.

PACS numbers: 72.20.Pa, 77.84.-s, 63.20.kg, 71.15.Mb

$\text{PbTiO}_3$  (PTO) is a well studied perovskite ferroelectric, and is used extensively in the technologically important ferroelectric/piezoelectric ceramic  $\text{PbZr}_x\text{Ti}_{(1-x)}\text{O}_3$  (PZT). PTO transitions from the cubic paraelectric (PE) phase to the tetragonal ferroelectric (FE) phase at temperature  $T_c = 763$  K. Recent computational work predicted PTO to be a promising *p*-type transparent conducting compound based on its electronic structure.<sup>1</sup> Following doping to increase electrical conductivity, we can speculate about its thermoelectric behavior. The thermoelectric figure of merit at temperature  $T$  is given by  $zT = \sigma S^2 T / (\kappa_L + \kappa_e)$ , where  $\sigma$  is the electrical conductivity,  $S$  is the Seebeck coefficient, and  $\kappa_L$  and  $\kappa_e$  are the lattice contribution and the electronic contribution to thermal conductivity. As a first approximation, the  $\kappa_e$  of semiconductors is related to  $\sigma$  as  $\kappa_e = L\sigma T$ . The Lorenz number  $L$  is a near-constant for many materials, which leaves little room for controlling  $\kappa_e$  independent of  $\sigma$ . On the other hand, researchers have been pursuing many methods to reduce  $\kappa_L$  to increase  $zT$ .<sup>2,3</sup>

PTO has a relatively small unit cell which may not favor low  $\kappa_L$ . However, it has been observed that anharmonicity, such as that seen in thermoelectrics like  $\text{PbTe}$ , can decrease  $\kappa_L$  despite small lattice constants. PTO is used in superlattices and alloys – morphologies that could enhance phonon scattering and thus reduce  $\kappa_L$  further. Despite this promise, only limited amount of experimental results are available on the topic of room-temperature and high-temperature behavior of  $\kappa_L$  in ferroelectrics including PTO.<sup>4–6</sup> Computational estimate of  $\kappa_L$  could illuminate some of these points. With this in mind, a semiclassical analysis of  $\kappa_L$ , as well as the electronic transport parameters of PTO are reported in this paper. The calculations are based on Boltzmann transport equations (BTE), which rely on *ab initio* results as the input. This study indicates a very low  $\kappa_L$  and high thermoelectric potential for PTO.

Here DFT-based lattice dynamics methods are applied to generate the second-order interatomic force constants (IFC2), which are then used in the BTE solver (for phonons) to determine  $\kappa_L$ . The lattice dynamics methods assume harmonic forces on the atoms. If the

forces have large anharmonic components, the resulting IFC2 will be less accurate, which in turn will make  $\kappa_L$  less precise. Thus, IFC2 from extreme anharmonic cases, or that from dynamically unstable structures cannot be used to determine the corresponding  $\kappa_L$ . For example, the cubic PTO structure for which DFT calculations predict imaginary phonon frequencies is outside the scope of the present study. However, tetragonal PTO (*t*- $\text{PbTiO}_3$ ) shows less anharmonicity under the same calculation methods, and hence provides an alternate route to study  $\kappa_L$  from first principles.

To understand if the degree of anharmonicity in *t*- $\text{PbTiO}_3$  is within a reasonable limit, I checked available experiments on PTO and other materials. The example of  $\text{PbTe}$ , an incipient ferroelectric and a leading thermoelectric, is particularly relevant in this context. Strong anharmonic interaction between longitudinal acoustic (LA) and transverse optic (TO) modes has been determined as the *cause* of the exceptionally low  $\kappa_L$  of  $\text{PbTe}$ .<sup>7,8</sup> DFT-based methods successfully estimated  $\kappa_L$  in  $\text{PbTe}$  despite such strong anharmonic interaction.<sup>9,10</sup> Anharmonicity in the phonon dispersion results of PTO has been studied experimentally.<sup>11–13</sup> By performing least-square analysis of the phonon frequencies near  $T_c$ , Freire and Katiyar concluded that anharmonicity in *t*- $\text{PbTiO}_3$  is small.<sup>14</sup> Taken together, the observations on  $\text{PbTe}$  and PTO validate the use of the DFT-based methods to determine  $\kappa_L$  for *t*- $\text{PbTiO}_3$ . Additionally, in this work the phonon dispersion and  $\kappa_L$  are computed for different tetragonal structures of *t*- $\text{PbTiO}_3$  to study how structural changes affect  $\kappa_L$ . This approach is similar to the recent work on  $\text{PbTe}$  and other Pb-chalcogenides by Skelton and co-workers.<sup>10</sup> Different *t*- $\text{PbTiO}_3$  structures show modest variation in  $\kappa_L$ , according to the calculations presented here; and the range of  $\kappa_L$  closely follows the experimental  $\kappa_L$ . This conclusion for PTO, and similar conclusions for  $\text{PbTe}$  and the related systems<sup>10</sup> suggest that the DFT-based determination of  $\kappa_L$  could be a robust method, applicable to other ferroelectric/antiferroelectric materials.

The DFT calculations presented in this work were performed with Vienna Abinitio Simulation Package (VASP).<sup>15,16</sup>

Local density approximation (LDA)-based projector-augmented wave (PAW) pseudopotentials,<sup>17</sup> which included the semicore  $p$  electrons of Ti, were used for these calculations. The self-consistent calculations (SCF) and ionic relaxations with fixed lattice parameters had a plane-wave cutoff of 400 eV, whereas a higher cutoff of 520 eV was applied when optimizing cell parameters. A  $8 \times 8 \times 8$  Monkhorst-Pack  $k$ -point mesh was used for the Brillouin zone integration. Forces on ions were converged to less than 0.001 eV/Å. Scalar relativistic effects were included in these calculations, but the spin-orbit effect was left out. According to these calculations, relaxed cell parameter for cubic PTO is  $a = 3.881$  Å. The optimized t-PbTiO<sub>3</sub> (referred to as the S<sub>2</sub> structure from now on) has  $a = 3.856$  Å, and  $c/a = 1.046$ . The cell parameters and the internal coordinates of atomic positions agree well with the previously reported values obtained from DFT-LDA calculations.<sup>18,19</sup> Electronic density of states (eDOS) of the optimized cubic and tetragonal structures were determined via non self-consistent calculations with a  $k$ -point grid of  $30 \times 30 \times 30$ . The top valence bands of PTO (both in tetragonal and cubic structures) show strong dispersive character and are formed by the hybridization between Pb  $6s^2$ - and O  $2p^6$ -like orbitals, whereas the bottom of the conduction bands are relatively flat and have large contribution from Ti  $3d$ -like orbitals. The eDOS calculated in this work agree with previous reports.<sup>1,20</sup>

Besides S<sub>2</sub>, the phonon dispersion and  $\kappa_L$  were determined for three other tetragonal structures, all with relaxed ionic positions. Two of these structures have  $a = 3.856$  Å with  $c/a = 1.06$  (S<sub>1</sub>) and 1.03 (S<sub>3</sub>), whereas the third structure has  $a = 3.904$  Å, and  $c/a = 1.03$  (S<sub>4</sub>). The systematic shift in phonon frequencies was studied using these tetragonal structures, by varying the lattice parameter  $a$  while the tetragonality ratio  $c/a$  was kept fixed, and vice versa. Phonon dispersion plots were computed under stringent convergence criteria, using the Phonopy code,<sup>21</sup> with VASP as the DFT calculator. A set of finite displacement calculations on the  $4 \times 4 \times 4$  supercells of t-PbTiO<sub>3</sub> (containing 320 atoms) produced the IFC2 used in this work.

Fig. 1 shows the phonon dispersion for the structures S<sub>1</sub>–S<sub>4</sub>. In this figure we zoom into the region with phonon frequencies up to 200 cm<sup>-1</sup> to inspect the thermal-current-carrying, low-lying phonon branches in greater detail. The acoustic modes of S<sub>4</sub> have smaller frequencies ("softer") than the rest, and those belonging to S<sub>1</sub>–S<sub>3</sub> nearly overlap except in the  $M$ – $\Gamma$  region, where the structures with smaller  $c/a$  have lower frequencies, i.e.,  $\omega(S_1) > \omega(S_2) > \omega(S_3)$ . Phonon frequencies of the lowest optic modes along the  $A$ – $M$ – $\Gamma$  path follow the same pattern for S<sub>1</sub>–S<sub>3</sub>, whereas the optic modes related to S<sub>4</sub> appear to have *higher* frequencies than S<sub>1</sub>–S<sub>3</sub>. The lowest optic mode at  $\Gamma$ , known as  $E(\text{TO}_1)$ ,<sup>22</sup> stiffens for structures that are more tetragonal. This effect of tetragonality on the zone-center  $E(\text{TO}_1)$  has been observed in previous calculations.<sup>19</sup> Experimental confirmation<sup>12</sup> of this trend

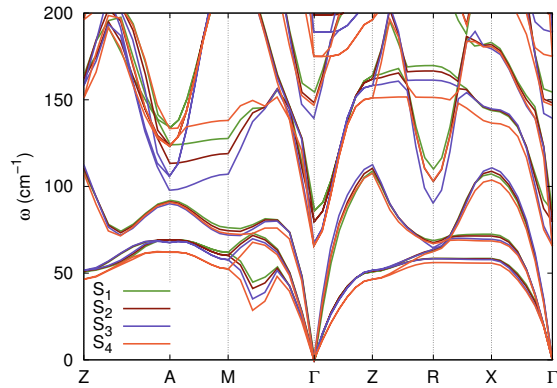


FIG. 1. (Color online) Lowest branches in the phonon dispersion for the structures S<sub>1</sub>–S<sub>4</sub>.

of  $E(\text{TO}_1)$  is available via the temperature behavior of t-PbTiO<sub>3</sub>: a rise in  $T$  that reduces the tetragonality in t-PbTiO<sub>3</sub> is found to lower the associated  $E(\text{TO}_1)$  frequency. Thus the experiments and the calculations agree qualitatively.<sup>23</sup>

In general, a more quantitative connection between structure and  $T$  can be determined in some cases using the quasiharmonic approximation (QHA), which includes the phonon contribution to Helmholtz free energy as a function of volume ( $V$ ) and  $T$ . Here we make a digression to look at the QHA analysis of t-PbTiO<sub>3</sub> before moving on to discuss  $\kappa_L$  calculations. QHA assumes harmonic forces on atoms at a specific volume, but allows for phonon frequencies to change with structure. Theoretical background and the implementation details of QHA are available in Refs. 10 and 24. Tetragonal symmetry in t-PbTiO<sub>3</sub> implies that the coefficient of thermal expansion (CTE), a second-rank tensor, has only two independent components, given by  $\alpha_{xx} (= \alpha_{yy})$  and  $\alpha_{zz}$  (following the Voigt notation). The components  $\alpha_{xx}$  and  $\alpha_{zz}$  are related to the principal components of strain as  $\epsilon_{xx} = \alpha_{xx}\Delta T$ , and  $\epsilon_{zz} = \alpha_{zz}\Delta T$ .<sup>25</sup> The volume CTE is  $\alpha_V = 2\alpha_{xx} + \alpha_{zz}$ . PTO shows negative thermal expansion (NTE) between  $\sim 300$  K– $T_c$ .<sup>26–28</sup> As  $T$  rises towards  $T_c$ , the  $c/a$  of t-PbTiO<sub>3</sub> decreases (as alluded to briefly in the last paragraph) while  $a$  increases slightly, with an overall reduction in volume. Past attempts at applying QHA to determine the thermal expansion in PTO have run into difficulties. In one case,  $\alpha_V$  came out to be positive,<sup>29</sup> whereas another study reported a vastly overestimated magnitude of  $\alpha_V$ .<sup>30</sup> In general, the lattice parameters of t-PbTiO<sub>3</sub> change in complex ways as functions of pressure,<sup>31–34</sup> which may be partly responsible for the difficulty in matching the QHA results for t-PbTiO<sub>3</sub> with the experimental CTE.

In this work, the directly comparable components of CTE would be those determined under epitaxial constraints, because the phonon dispersion of different tetragonal structures (S<sub>1</sub>–S<sub>4</sub>) were compared by changing either the in-plane ( $x$  and  $y$ ) or the out-of-plane ( $z$ )

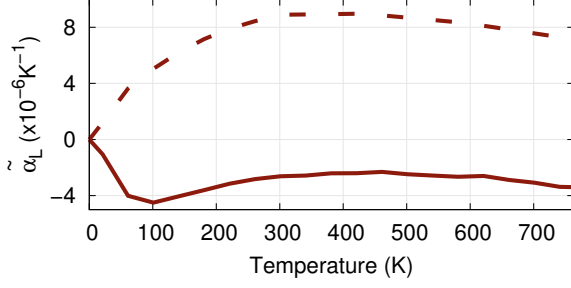


FIG. 2. CTE components for t-PbTiO<sub>3</sub> as a function of temperature. The solid (lower) and the dashed (upper) curves represent  $\tilde{\alpha}_{zz}$  and  $\tilde{\alpha}_{xx}$ , respectively.

lattice direction(s), while holding the other fixed. The resulting CTE components can be termed *clamped* coefficients,  $\tilde{\alpha}_{xx}$  and  $\tilde{\alpha}_{zz}$ , which are not the same as  $\alpha_{xx}$  and  $\alpha_{zz}$ . The Phonopy-QHA code<sup>21</sup> was used to compute  $\tilde{\alpha}_{xx}$  and  $\tilde{\alpha}_{zz}$ . To determine  $\tilde{\alpha}_{xx}$ , a total of 12 structures were studied which spanned a variation in  $a$  by  $\pm 0.5\%$  around the optimized  $a$  of t-PbTiO<sub>3</sub> (while the optimized  $c$  was held fixed). Similarly,  $\tilde{\alpha}_{zz}$  was obtained using 11 structures by varying  $c$  in a range of  $-0.3\%$  to  $0.7\%$  around the optimized  $c$ , while  $a$  remained fixed. In Fig. 2 we see that in the 300 K–600 K,  $\tilde{\alpha}_{xx}$  is  $\sim 9 \times 10^{-6} \text{ }^\circ\text{C}^{-1}$  and  $\tilde{\alpha}_{zz}$  is  $\sim -3 \times 10^{-6} \text{ }^\circ\text{C}^{-1}$ . The phonon dispersion results for S<sub>1</sub>–S<sub>4</sub> structures along with the computed values of  $\tilde{\alpha}_{xx}$  and  $\tilde{\alpha}_{zz}$  firmly establish that the structures with smaller  $c/a$  ratio correspond to higher  $T$  in these calculations.

Having explored how the S<sub>1</sub>–S<sub>4</sub> structures relate to  $T$ , we now proceed to the results of the  $\kappa_L$  calculations. The ShengBTE code<sup>35</sup> used in this work iteratively solves BTE for phonons to determine  $\kappa_L$ . The IFC2 required in this code were obtained using the Phonopy code as described earlier, generated with  $4 \times 4 \times 4$  supercells via finite difference approach. The anharmonic IFC3 were obtained using the code `thirdorder.py`<sup>36</sup> (supplied with ShengBTE), following the same finite difference methods on  $3 \times 3 \times 3$  t-PbTiO<sub>3</sub> supercells. Interaction up to the third nearest neighbors was included in these calculations, and VASP was used as the DFT engine. The linearized BTE was solved on a  $\Gamma$ -centered,  $16 \times 16 \times 16$   $q$ -point grid, which sufficiently converged  $\kappa_L$ . The supercells considered above to generate the set of IFC2 and IFC3 adequately converged  $\kappa_L$ . To test the convergence of  $\kappa_L$  on supercell size, additional sets of IFC2 and IFC3 were generated for the S<sub>2</sub> structure, on supercells of dimensions  $3 \times 3 \times 3$  and  $2 \times 2 \times 2$ , respectively. Including the original choice ( $4 \times 4 \times 4$  supercells for IFC2, and  $3 \times 3 \times 3$  supercells for IFC3), four combinations of IFC2 and IFC3 were tested. For S<sub>2</sub>,  $\kappa_L$  calculated with these four combinations lie within  $0.2 \text{ Wm}^{-1}\text{K}^{-1}$ , accurate enough for the purpose of this work.

Fig. 3 shows the  $\kappa_L$  values for the structures S<sub>1</sub>–S<sub>4</sub>, with the shaded region corresponding to extrapolated values of  $\kappa_L$  for  $T > T_c$ . First, we note that  $\kappa_L$  in PTO is low, especially at high temperature, and the structures

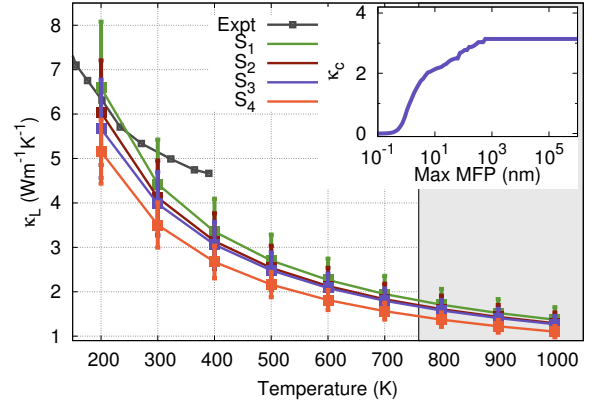


FIG. 3. (Color online)  $\kappa_L$  as a function of  $T$  for the S<sub>1</sub>–S<sub>4</sub> structures of t-PbTiO<sub>3</sub>, along with the experimental data from Ref. 6. The upper bound and the lower bound of the bars represent the  $\kappa_L$  values along the in-plane and the out-of-plane axes, whereas the solid line represents one-third the trace of  $\kappa_L$ . The extrapolated region (for  $T > T_c$ ) is shaded in grey. Cumulative  $\kappa_L$  is expressed as a function of maximum mean free path for the S<sub>2</sub> structure (inset).

with smaller  $c/a$  show a lower  $\kappa_L$ . This effect is most pronounced for S<sub>4</sub>, whereas the curves corresponding to S<sub>1</sub>–S<sub>3</sub> show significant overlap. The structural dependence of  $\kappa_L$  in t-PbTiO<sub>3</sub> indicates that anharmonicity strongly affects  $\kappa_L$ . The experimental thermal conductivity results on perovskite ferroelectric samples<sup>4,6</sup> suggest that structural phase transitions do not significantly change the overall  $T$  dependence of  $\kappa_L$ , except for a discontinuity close to  $T_c$ . This observation was used to calculate  $\kappa_L$  beyond  $T_c$  using IFC2 and IFC3 corresponding to tetragonal structures. The top and the bottom end of the bars in Fig. 3 correspond to the  $\kappa_L$  values along the in-plane and the out-of-plane axes respectively, while the solid line represents the one-third the trace of the  $\kappa_L$  tensor. The inset of Fig. 3 shows the cumulative  $\kappa_L$  as a function of the maximum phonon mean free path for the optimized t-PbTiO<sub>3</sub> structure (S<sub>2</sub>) at 400 K. According to these calculations, a nanoparticle of 10 nm diameter will have  $\kappa_L$  of about  $2 \text{ Wm}^{-1}\text{K}^{-1}$  – two thirds of its saturation value. Thus nanostructuring PTO may provide another route to reduce  $\kappa_L$  on top of its already low  $\kappa_L$ .

A comparison with the available experimental data for PTO shows overall agreement,<sup>6</sup> although the computed  $\kappa_L$  appears underestimated in the 250 K–400 K. Experimental results include  $\kappa_e$ , partly explaining the difference. Another contribution to this mismatch may be due to ignoring the spin-orbit effect in the calculations, reported to be important in certain cases.<sup>9</sup> A third source of the difference could be a result of using harmonic approximation to calculate the phonon dispersion, which predicted (spuriously) smaller frequencies for the low-lying TO modes. This may have assigned a larger fraction of the thermal current to the TO modes in the present calculations. The optic modes in general have slower group velocity. Thus, a bigger fraction of the heat current car-

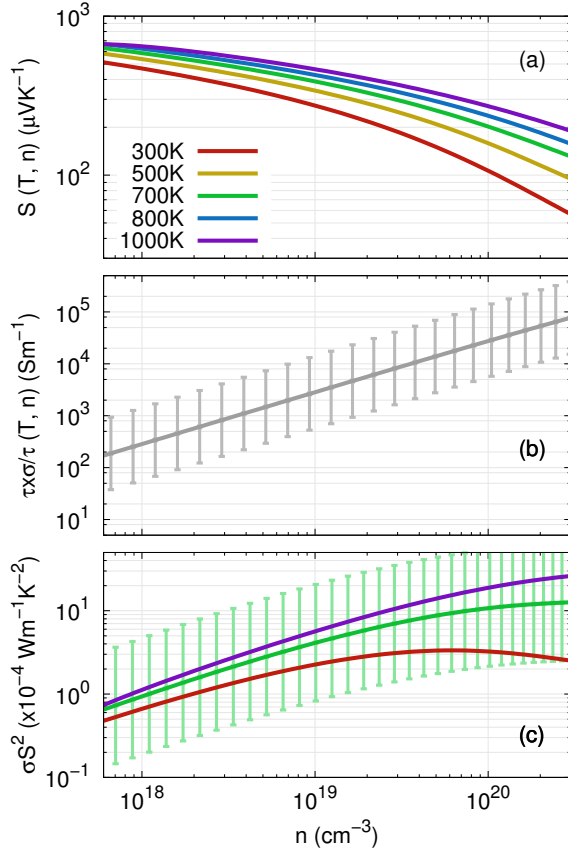


FIG. 4. (Color online) Calculated thermoelectric parameter values: (a)  $S(T, n)$  for five temperatures, (b)  $\sigma/\tau \times \tau$  for three representative values of  $\tau$ : The solid line, and the upper and the lower limits of the vertical bars represent 5 fs, 25 fs, and 1 fs, respectively. (c) Power factor  $\sigma S^2$  for systems at 300 K, 700 K, and 1000 K. The bars represent the same range of  $\tau$  as in panel (b) for the 700 K curve [Same legends as (a)].

ried by optic modes would lower  $\kappa_L$  overall.<sup>37</sup> A conclusive insight would require observations from more experiments, and calculations that consider anharmonicity explicitly.

Low  $\kappa_L$  predicted for t-PbTiO<sub>3</sub> would make it a promising thermoelectric candidate if its electronic transport properties are good enough. To this end, semiclassical Boltzmann theory-based BoltzTraP<sup>38</sup> code was used to estimate  $S$ ,  $\sigma$ , and  $\kappa_e$ , within the constant scattering time approximation (CSTA). In CSTA,  $\sigma$  and  $\kappa_e$  are determined within a factor of the scattering time  $\tau$ , considered a parameter, whereas  $S$  has no such dependence on  $\tau$ . Experimental results on  $\sigma$ , mobility and carrier concentration can be used to approximate  $\tau$ . However, such experimental results are lacking for conductive samples of PTO. As a substitute, a broad range of  $\tau$ , from 1 fs ( $=10^{-15}$  s) to 25 fs, was used in these calculations.

Fig. 4(a)-(c) show the calculated values of  $S$ ,  $\sigma/\tau$ , and the power factor  $\sigma S^2$ , all presented as functions of the carrier density  $n$ . In these calculations  $\kappa_e$  was found to

be small ( $\leq 0.5 \text{ W m}^{-1} \text{ K}^{-1}$  with  $\tau = 5 \text{ fs}$ ) compared to  $\kappa_L$ , and hence ignored in further discussions. The DFT-derived eDOS were obtained from the cubic or the tetragonal structure, for  $T \geq T_c$  and  $T < T_c$ , respectively; and were interpolated by a factor of 100 for the transport calculations. For the t-PbTiO<sub>3</sub> structure, one-third the trace of the  $S$  and the  $\sigma$  tensors are presented. As is widely observed for semiconductor thermoelectrics,  $S$  increases with  $T$  (for the same  $n$ ), and drops with increasing  $n$  (calculated at the same  $T$ ). The  $\sigma/\tau$  curve has no  $T$  dependence, and in panel (b) we see a representative curve, with the bars spanning a region bound by  $\tau = 25 \text{ fs}$  as the upper limit, to  $\tau = 1 \text{ fs}$  as the lower limit. The solid line is drawn with  $\tau = 5 \text{ fs}$ . Fig. 4(c) shows the estimated values of the power factor, which carries over the uncertainty in  $\tau$  (the range of  $\tau$  shown only for the  $T = 700 \text{ K}$  case, the rest drawn for  $\tau = 5 \text{ fs}$  only). This plot indicates that  $\sigma S^2$  is often greater than  $0.002 \text{ W m}^{-1} \text{ K}^{-2}$  for a wide range of values of  $\tau$  and  $n$ . For reference, a power factor of  $0.002 \text{ W m}^{-1} \text{ K}^{-2}$  at 1000 K, accompanied by the estimated  $\kappa_L$  value of  $1.15 \text{ W m}^{-1} \text{ K}^{-1}$ , indicates a  $zT$  of 1.7 – highly promising as an initial estimate.

To summarize this work, the calculations presented here predict very low  $\kappa_L$  for PTO, influenced by the anharmonicity. The results largely agree with experiments. The low  $\kappa_L$  and the accompanying favorable electronic transport values indicate great promise of PTO as a thermoelectric material, provided the electrical conductivity is raised by doping. PTO and related perovskite functional materials have been synthesized and characterized in a variety of morphologies and compositions. Thus, processes such as alloying or increasing the complexity of the unit cell, among other measures, could be utilized to further reduce  $\kappa_L$ . Synthesizing PTO in disordered structure may provide another route to reduce  $\kappa_L$  while maintaining high  $\sigma$ . The top of the valence band of PTO is formed by the hybridization between the Pb 6s and the O 2p orbitals. The expansive, anisotropic Pb 6s orbitals may allow band-like hole conduction even in the absence of crystalline order, an idea originally suggested in the context of  $n$ -type amorphous transparent conducting oxides.<sup>39</sup> This idea has recently been proposed as a means to reduce  $\kappa_L$  in ZnO-based  $n$ -type thermoelectrics.<sup>40</sup> The present work demonstrates that  $\kappa_L$  can be computed for the low-symmetry, dynamically stable phases of ferroelectric/antiferroelectric materials, which can then be extended by reasonable approximation to high- $T$  regime. Comparison with experiments show that this approach can be a practical way to estimate  $\kappa_L$  on dynamically unstable systems which are otherwise intractable.

*The calculations related to this work will be available for download after the peer-review process.*

## ACKNOWLEDGMENTS

The author is grateful to Michael L. Falk for the discussions and the support, to Jesús Carrete for the discus-

sions regarding the implementation of ShengBTE, and to Olivia Alley for the suggestions on the manuscript. The work was supported by NSF grant DUE-1237992. This project used the computational resources of Extreme Sci-

ence and Engineering Discovery Environment (XSEDE), which is supported by NSF grant number ACI-1053575; and The Maryland Advanced Research Computing Center (MARCC) supported by the State of Maryland.

- 
- \* aroy21@jhu.edu
- <sup>1</sup> G. Hautier, A. Miglio, G. Ceder, G.-M. Rignanese, and X. Gonze, *Nat. Commun.* **4**, 2292 (2013).
  - <sup>2</sup> G. J. Snyder and E. S. Toberer, *Nat. Mater.* **7**, 105 (2008).
  - <sup>3</sup> M. W. Gaultois and T. D. Sparks, *Appl. Phys. Lett.* **104**, 113906 (2014).
  - <sup>4</sup> A. J. H. Mante and J. Volger, *Phys. Lett. A* **24**, 139 (1967).
  - <sup>5</sup> B. A. Strukov and A. A. Belov, *Phase Transitions* **51**, 175 (1994).
  - <sup>6</sup> M. Tachibana, T. Kolodiaznyi, and E. Takayama-Muromachi, *Appl. Phys. Lett.* **93**, 092902 (2008).
  - <sup>7</sup> J. An, A. Subedi, and D. Singh, *Solid State Commun.* **148**, 417 (2008).
  - <sup>8</sup> O. Delaire, J. Ma, K. Marty, A. F. May, M. A. McGuire, M.-H. Du, D. J. Singh, A. Podlesnyak, G. Ehlers, M. D. Lumsden, and B. C. Sales, *Nat. Mater.* **10**, 614 (2011).
  - <sup>9</sup> Z. Tian, J. Garg, K. Esfarjani, T. Shiga, J. Shiomi, and G. Chen, *Phys. Rev. B* **85**, 184303 (2012).
  - <sup>10</sup> J. M. Skelton, S. C. Parker, A. Togo, I. Tanaka, and A. Walsh, *Phys. Rev. B* **89**, 205203 (2014).
  - <sup>11</sup> G. Shirane, J. D. Axe, J. Harada, and J. P. Remeika, *Phys. Rev. B* **2**, 155 (1970).
  - <sup>12</sup> G. Burns and B. A. Scott, *Phys. Rev. B* **7**, 3088 (1973).
  - <sup>13</sup> C. M. Foster, Z. Li, M. Grimsditch, S.-K. Chan, and D. J. Lam, *Phys. Rev. B* **48**, 10160 (1993).
  - <sup>14</sup> J. D. Freire and R. S. Katiyar, *Phys. Rev. B* **37**, 2074 (1988).
  - <sup>15</sup> G. Kresse and J. Furthmüller, *Phys. Rev. B* **54**, 11169 (1996).
  - <sup>16</sup> G. Kresse and D. Joubert, *Phys. Rev. B* **59**, 1758 (1999).
  - <sup>17</sup> P. E. Blöchl, *Phys. Rev. B* **50**, 17953 (1994).
  - <sup>18</sup> A. García and D. Vanderbilt, *Phys. Rev. B* **54**, 3817 (1996).
  - <sup>19</sup> P. Marton and J. Hlinka, *Phase Transitions* **86**, 200 (2013).
  - <sup>20</sup> S. Piskunov, E. Heifets, R. Eglitis, and G. Borstel, *Comput. Mater. Sci.* **29**, 165 (2004).
  - <sup>21</sup> A. Togo and I. Tanaka, *Scr. Mater.* **108**, 1 (2015).
  - <sup>22</sup> Conventional terminology, based on the decomposition of vibrational representation at  $\Gamma$ . See Ref. 18 for details.
  - <sup>23</sup> In real life, strong anharmonic forces associated with the ferroelectric transition renormalize the phonon frequencies to real values, as PTO transitions to cubic structure.
  - <sup>24</sup> S. Baroni, S. De Gironcoli, A. Dal Corso, and P. Gianozzi, *Rev. Mod. Phys.* **73**, 515 (2001).
  - <sup>25</sup> J. F. Nye, *Physical properties of crystals: their representation by tensors and matrices* (Oxford university press, 1985).
  - <sup>26</sup> G. Shirane, S. Hoshino, and K. Suzuki, *Phys. Rev.* **80**, 1105 (1950).
  - <sup>27</sup> G. Shirane and S. Hoshino, *J. Phys. Soc. Jpn.* **6**, 265 (1951).
  - <sup>28</sup> J. Chen, X. Xing, R. Yu, and G. Liu, *J. Am. Ceram. Soc.* **88**, 1356 (2005).
  - <sup>29</sup> L. Wang, P. Yuan, F. Wang, E. Liang, Q. Sun, Z. Guo, and Y. Jia, *Mater. Res. Bull.* **49**, 509 (2014).
  - <sup>30</sup> F. Wang, Y. Xie, J. Chen, H. Fu, and X. Xing, *Appl. Phys. Lett.* **103**, 221901 (2013).
  - <sup>31</sup> S. Tinte, K. M. Rabe, and D. Vanderbilt, *Phys. Rev. B* **68**, 144105 (2003).
  - <sup>32</sup> J. Frantti, Y. Fujioka, and R. M. Nieminen, *J. Phys. Chem. B* **111**, 4287 (2007).
  - <sup>33</sup> P. Ganesh and R. E. Cohen, *J. Phys. Condens. Matter* **21**, 064225 (2009).
  - <sup>34</sup> J. Zhu, J. Zhang, H. Xu, S. C. Vogel, C. Jin, J. Frantti, and Y. Zhao, *Sci. Rep.* **4** (2014).
  - <sup>35</sup> W. Li, J. Carrete, N. A. Katcho, and N. Mingo, *Comp. Phys. Commun.* **185**, 1747 (2014).
  - <sup>36</sup> W. Li, L. Lindsay, D. A. Broido, D. A. Stewart, and N. Mingo, *Phys. Rev. B* **86**, 174307 (2012).
  - <sup>37</sup> E. S. Toberer, L. L. Baranowski, and C. Dames, *Annu. Rev. Mater. Res.* **42**, 179 (2012).
  - <sup>38</sup> G. K. H. Madsen and D. J. Singh, *Comput. Phys. Commun.* **175**, 67 (2006).
  - <sup>39</sup> H. Hosono, *J. Non-Cryst. Solids* **352**, 851 (2006).
  - <sup>40</sup> A. Roy, Y.-T. Cheng, and M. L. Falk, Unpublished.